JOURNAL OF AIRCRAFT
Vol. 35, No. 4, July–August 1998

Nonlinear Model for Aircraft Brake Squeal Analysis: Model Description and Solution Methodology

Steven Y. Liu,* James T. Gordon,† and M. Akif Özbek‡
The Boeing Company, Seattle, Washington 98124

A model is presented for the analysis of primary squeal-mode vibration in aircraft braking systems. The destabilizing mechanism in the model utilizes nonlinear mechanical and material surface properties of the brake heat stack to couple lateral translation and yaw of the rotors and stators. Geometric and stiffness properties of the brake and landing-gear structure couple piston-housing torsional rotation and axle fore–aft bending with lateral translation and yaw of the heat stack. The model does not use brake negative damping and it predicts that system instability can occur with a constant brake-friction coefficient as has been observed on both dynamometer and flight tests. System stability can be altered by changes in the brake-friction coefficient, pressure, stiffness, geometry, and various brake-design parameters. Enhanced versions of the model are presented that include a more detailed structural representation of the piston-housing torque tube and the hydraulic flow equations for each piston. The model is extended to a fore–aft wheel pair on a two-axle, main-landing gear truck. Stability is investigated by determining eigenvalues of the linearized perturbation equations about each steady-state operating point of the nonlinear system. The nonlinear dynamic equations are integrated numerically to obtain time-history responses. Results from stability analyses and parametric studies using this model are presented in a companion paper.

Nomenclature

A_k = $\pi(R_o^k - R_i^k)$, $k = 2, 3, 4, 5, 6$, $(\text{in.})^k$
B_x = $(x_{s0} - x_{r0})$, in.
B_ϕ = $(\phi_{s0} - \phi_{r0})$, rad
C_{lug} = lug fore–aft damping coefficient, lb/in./s
C_{wk} = wheel key yaw damping, lb-in./rad/s
C_{xr} = rotor lateral translational damping, lb/in./s
C_{xs} = stator lateral translational damping, lb/in./s
C_{yax} = axle fore–aft deflection-damping coefficient, lb/in./s
C_θ = piston-housing torsional damping, lb-in./rad/s
$C_{\phi\text{ax}}$ = axle-bending rotation-damping coefficient, lb-in./rad/s
$C_{\phi r}$ = rotor yaw viscous damping, lb-in./rad/s
$C_{\phi s}$ = stator yaw viscous damping, lb-in./rad/s
d_e = brake-rod lateral offset, in.
F_{drag} = tire–ground drag load, lb
F_{hyd} = lateral force (brake pressure), lb
F_n = rotor/stator contact force, lb
$\hat{F}_n$ = rotor/stator contact stress, lb/in.^{2}
F_{rod} = brake-rod axial load, lb
F_t = tangential force, lb
$\hat{F}_t$ = tangential stress, lb/in.^{2}
I_{axle} = axle moment of inertia, lb-in.-s^2
I_w = wheel inertia, lb-in.-s^2
I_θ = stator polar moment of inertia, lb-in.-s^2
$I_{\phi r}$ = yaw polar moment of inertia, lb-in.-s^2
$I_{\phi s}$ = yaw polar moment of inertia, lb-in.-s^2
K_{lug} = center-lug fore–aft stiffness, lb/in.
K_{rod} = brake-rod axial stiffness, lb/.in.
K_{rr} = lateral stiffness of rotor (caused by backing plate), lb/in./rad
K_{wk} = yaw stiffness of wheel key, lb-in./rad
K_θ = piston-housing torsional stiffness, lb-in./rad
$K_{\phi r}$ = rotor yaw stiffness (caused by backing plate), lb-in./rad
$K_{\phi s}$ = stator yaw stiffness, lb-in./rad
K_{11} = axle-bending $y - y$ stiffness, lb/in.
K_{12} = axle-bending $y - \phi$ stiffness, lb/rad
K_{21} = axle-bending $y - \phi$ stiffness, K_{12}, lb/rad
K_{22} = axle-bending $\phi - \phi$ stiffness, lb-in./rad
M_b = yaw moment, lb-in.
m_{axle} = axle mass, lb-s^2/in.
m_{lug} = center-lug mass, lb-s^2/in.
m_r = rotor mass, lb-s^2/in.
m_s = stator mass, lb-s^2/in.
N = number of brake stages, nondimensional
P_{net} = net-brake hydraulic pressure, lb/in.^{2}
p_i = hydraulic pressure at piston i, lb/in.^{2}
p_0 = inlet pressure, lb/in.^{2}
Q_0 = inlet flow, in.^{3}/s
R_b = piston-housing bushing radius, in.
R_e = distance axle to brake-rod axis, in.
R_i = friction surface inner radius, in.
R_o = friction surface outer radius, in.
R_r = rolling radius of tire, in.
R_w = wheel radius, in.
r = radius (integration variable), in.
r_{eff} = friction-material effective radius, in.
S = tire slip ratio, nondimensional
$\dot{S}_i$ = brake piston i stroking rate, in./s
T = brake torque, lb-in.
V_{ij} = fluid velocity between pistons i and j, in./s
v = aircraft ground speed, in./s
W = aircraft weight per wheel, lb
x_r = rotor lateral displacement, in.
x_s = stator lateral displacement, in.
y_{axle} = axle fore–aft bending, in.
y_{lug} = lug fore–aft deflection, in.
θ = angle (integration variable), rad
θ_s = piston-housing torsional rotation, rad

Presented as Paper 96-1251 at the AIAA Dynamic Specialist Conference, Salt Lake City, UT, April 18–19, 1996; received July 29, 1996; revision received Jan. 26, 1998; accepted for publication Jan. 26, 1998.

*Principal Engineer, Structures Vibration Technology.
†Senior Principal Engineer, Structures Vibration Technology. Senior Member AIAA.
‡Senior Specialist Engineer, Structures Vibration Technology. E-mail: akif.ozbek@boeing.com. Member AIAA.

μ_{brk} = brake-material friction coefficient, nondimensional
μ_{grd} = ground-friction coefficient, nondimensional
μ_{ph} = piston-housing bushing-friction coefficient, nondimensional
μ_r = rotor–wheel key friction coefficient, nondimensional
μ_s = stator–spline friction coefficient, nondimensional
ϕ_{axle} = axle bending rotation, rad
ϕ_r = rotor yaw rotation, rad
ϕ_s = stator yaw rotation, rad
Ω_w = wheel rotation, rad/s

I. Introduction

A TYPICAL aircraft landing-gear braking system and its components are shown in Fig. 1. The brake assembly consists of a torque tube, rotors, stators, piston housing, brake rod, and hydraulic system. The brake is activated by hydraulic pressure causing the pistons to push against the first stator, which compresses the heat stack (rotors and stators). Friction between the rotors and stators dissipates the kinetic energy as heat. Rotors are connected to the wheels by beam keys that are inserted into slots on the rotor outer radius. Stators are fitted over torque-tube splines by slots on the stator inner radius. The brake torque is transmitted from the torque tube and piston-housing arm through the brake rod to the landing-gear structure.

In recent years, the use of carbon brakes on large civilian aircraft has increased largely as a result of the superior performance of carbon over traditional materials. In addition to offering considerable weight savings when compared with steel, carbon has a higher friction coefficient, a higher specific heat, and a better wear rate. However, it is also known that carbon brakes are prone to vibrate.

A. Brake Vibration Categories

Braking-system vibrations are generally categorized as gear walk, whirl, squeal, chatter, or rotor-cycloidal motion. *Gear walk* is the low-frequency (5–20 Hz) fore–aft motion of the landing-gear assembly. This motion is caused by tire–runway interface friction loads that deflect the landing gear. It may sometimes be induced by the antiskid system, and could cause passenger discomfort.

Whirl is the wobbling motion of the brake's rotating parts against its stationary parts. It usually occurs at high ground speed with frequencies in the 200–400-Hz range. This mode is highly destructive and could cause carbon chipping or cracking, piston-housing ovalization, fracture of inserts, and heat-shield damage. Whirl is caused by the high-friction coefficient of the brake material and can be detected by the phasing of pressure oscillations among adjacent pistons. A common remedy for whirl is to insert orifices between pistons or fluid blocks in the hydraulic passageways.

Rotor-cycloidal motion is the radial and rotational motion of the heat stack coupled with stack-axial breathing motion. It usually occurs at low brake pressure when wear lip formations have developed. It can be prevented by introducing grooves on the stators at the rotor i.d. and on the rotors at the stator o.d.

Chatter is characterized by torsional oscillations of the wheel and rotating brake parts about the axle restrained by the elasticity of the tire. The chatter frequency is typically between 50 and 100 Hz and can be coupled with squeal modes.

Squeal can be defined as the torsional oscillations of the nonrotating brake components about the axle. The squeal modes have a frequency spectrum of 100–10,000 Hz and are caused by the characteristics of the brake-friction material. Squeal can produce very high oscillatory loads on the landing gear and brake structure and can sometimes cause brake failure. Possible solutions are to add damping at appropriate locations, change the brake-friction material properties, and modify component stiffnesses or geometry.

B. Primary Squeal-Mode Description

Flight-test data (Fig. 2) have shown that two primary squeal modes are responsible for producing the high-amplitude oscillatory loads in main landing-gear components occasionally encountered during landing and taxiing. The lower-frequency mode has the axles and brakes vibrating in-phase in the 140–160-Hz range. This mode is significant because the dynamic loads are additive on the center lug that is the attachment point for the two brake rods on each side of the truck to the lower oleo. The higher-frequency mode is characterized by the axles and brakes vibrating out of phase in the 180–250-Hz range. For this mode, the dynamic loads are subtractive on the center lug. Typically, the out-of-phase mode is predominant, although both have been encountered. Other squeal modes can exist, either singly or in combinations, depending on the system-parameter values. The following are some phenomena observed during testing:

1) Vibration occurs erratically and is not repeatable.
2) Vibration can occur at all taxiing and landing speeds.
3) Vibration usually occurs at low hydraulic pressures.

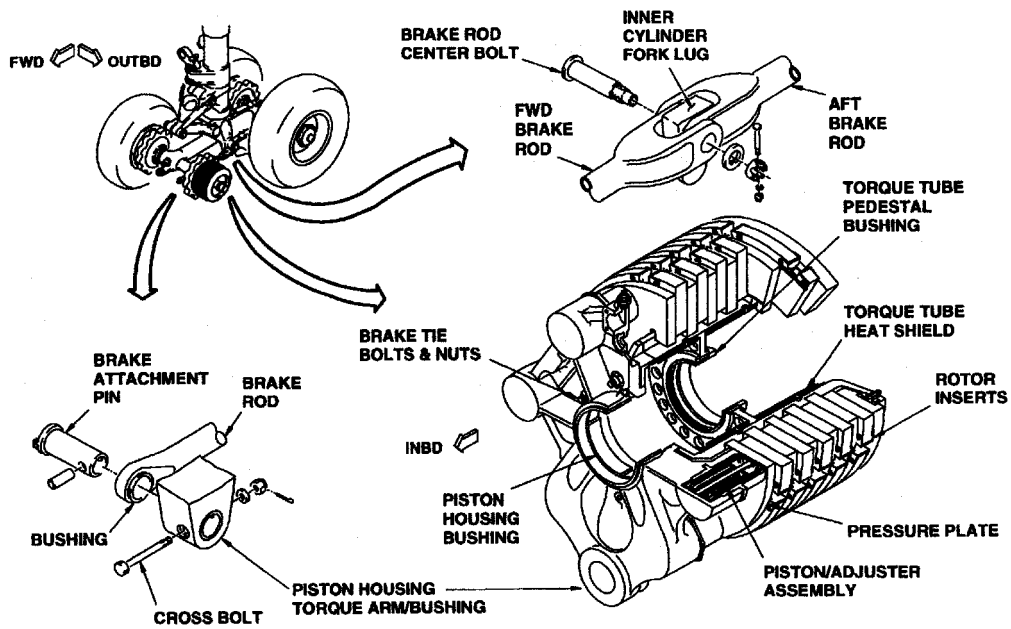

Fig. 1 Typical two-axle gear configuration.

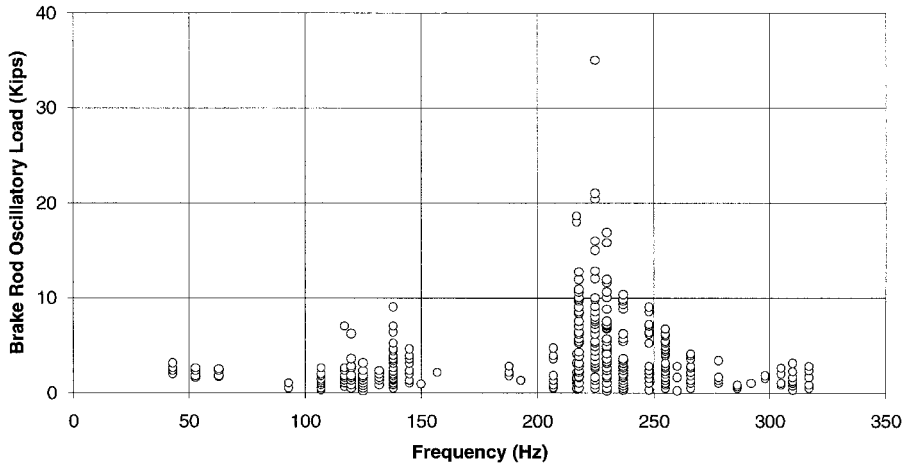

Fig. 2 Flight-test rod load vs squeal frequency.

4) Vibration characteristics are affected by brake structural design.

The first observation suggests that the vibration is related to the friction-material properties, whereas the remaining observations are related to the mechanical properties of the brake system.

C. Analysis of Squeal Vibrations

Analyses of squeal phenomena have used one of four general mechanisms for friction-induced system instability: 1) stick-slip, 2) variable dynamic-friction coefficient, 3) Sprag-slip, and 4) geometric coupling. The first two approaches rely on changes in the friction coefficient with relative sliding speed to affect system stability. The latter two approaches utilize kinematic constraints and modal coupling to develop the squeal instability when the friction coefficient is constant.

Stick-slip is a low sliding-speed phenomenon caused by the static-friction coefficient being higher than the dynamic coefficient. The variable dynamic-friction coefficient approach relies on a negative slope of the friction coefficient vs sliding-speed relationship to cause the self-excited instability. Earles and Soar[1] discussed these four types of friction-induced instabilities and presented an experimental and analytical study of squeal in pin–disk-type brakes. Their analytical model included simple single-degree-of-freedom models for the translation and torsional freedoms to investigate coupling effects. Their torsional model included nonlinear damping effects in the torsional freedom.

Ibrahim[2,3] presented a comprehensive literature review of the mechanics of friction-induced vibrations including chatter and squeal. Tworzydlo et al.[4] also presented a review of work in this field.

Millner[5] presented an analysis of disk-brake squeal that utilized a linear model having modal coupling between a single pad and disk to produce instability for a constant friction coefficient. Millner's results showed that system stability was affected primarily by changes in the friction coefficient, the Young's modulus of the pad material, caliper stiffness, and geometry.

D. Aircraft Squeal-Analysis Methods

The brake-friction coefficient is a poorly defined, highly nonlinear time-dependent function of pressure, temperature, relative velocity of the friction surfaces, etc. A common approach for analyzing squeal vibration on aircraft brakes is to use the concept of negative damping as the fundamental destabilizing mechanism. Equation (1) is a typical example of a single-degree-of-freedom model utilizing negative damping to simulate the primary brake-squeal mode

$$I_\theta \ddot{\theta} + C_\theta \dot{\theta} + K_\theta \theta = 2N\mu_{\text{brk}} A_p P_{\text{net}} r_{\text{eff}} \tag{1}$$

θ is the torsional rotation of the brake stationary parts about the axle, and dots over symbols indicate differentiation with respect to time t. I_θ, C_θ, and K_θ are the inertia, damping, and stiffness of the brake stationary parts about the axle, respectively. C_θ is an equivalent viscous-damping coefficient representing the Coulomb friction at the piston-housing bushings. K_θ is the torsional stiffness about the axle caused by the brake rod. $K_\theta = R_e^2 K_{\text{rod}}$, where R_e is the distance from the axle centerline to the brake-rod's axis, and A_p is the net piston area.

The linearized friction coefficient about a point μ_0 has the functional form

$$\mu_{\text{brk}} = \mu_0 - \mu_{\text{nd}}(\Omega_w - \dot{\theta}) \tag{2}$$

where Ω_w is the rotational speed of the wheel and is assumed to be constant. μ_0 and μ_{nd} are positive quantities. Forming the characteristic equation and examining its roots shows that the real part of the eigenvalue is $(-C_\theta + 2N\mu_{\text{nd}} A_p P_{\text{net}} r_{\text{eff}})/2I_\theta$. When this quantity becomes positive, the system is unstable.

The phenomenon of friction coefficient varying with relative velocity has been observed in some materials, and this approach has been widely used in analyzing brake squeal. However, there are several major deficiencies with this approach when analyzing aircraft carbon brakes. Firstly, no data indicate that the brake-friction coefficient has a strong functional dependence on relative speed between the rotor and stator contact surfaces. In fact, test data show that during a squeal-vibration event the brake-friction coefficient is essentially a constant. Secondly, model predictions using brake negative damping do not agree with test results. For example, test data indicate that braking system dynamic stability increases with increasing brake hydraulic pressure. Models using negative damping predict the opposite trend, showing decreased stability with increasing pressure. Test data also have a bell-shaped distribution with squeal frequency as shown in Fig. 2. The frequencies of unstable modes predicted by models using negative damping essentially do not vary with changing pressure, friction coefficient, etc. Thus, the goal of this paper is to develop a realistic model that does not have these deficiencies and that agrees with the experimental observations described previously.

II. Model Description

For a single-wheel model, the degrees of freedom are rigid-body lateral displacement and yaw of the rotor and stator (x_r, ϕ_r and x_s, ϕ_s, respectively); θ_s; y_{axle}; ϕ_{axle}; and Ω_w.

For the fore–aft wheel-pair model, the single-wheel freedoms are included for each wheel plus the fore–aft deflection of the center lug y_{lug} on the landing gear lower oleo strut.

Additional degrees of freedom required for the brake-hydraulic equations, which are presented in Appendix A, are the piston pressure p_i at each piston, the fluid velocity v_{ij} between

two adjacent piston cavities, and the piston-housing axial deflection x_{iph} at each piston.

A. Assumptions

The coefficient μ_{brk} is assumed to be a constant when squeal vibrations occur. For simplicity, the multistage brake is represented by a single rotor and stator. It is assumed that the rotor and stator friction surfaces are always in contact. However, the validity of the model is not restricted to these assumptions.

The relative displacement between the rotor and stator is assumed to be a function of rotor and stator rigid-body lateral translation and yaw. The normal contact force at the rotor and stator interface is represented by a cubic polynomial in the relative displacement and velocity between the rotor and stator in compression. The nonlinear relationship between load and deflection have been verified by static tests conducted on complete brake heat-stack assemblies and small-scale coupons.

The brake-rod axial load is assumed to be a function of the piston-housing torsional and yaw rotations plus the axle- and center-lug fore–aft deflections.

B. Nonlinear Contact Stress

Assume that the nonlinear normal stress $\hat{F}_n$ acting at the interface surface between a rotor and stator can be expressed as a polynomial in the relative displacement and velocity normal to the friction surface. Then $\hat{F}_n$ is given by

$$\hat{F}_n = \sum_{i=0}^{m} [K_i x^i + C_i \dot{x}^i] \tag{3}$$

where, x and $\dot{x}$ are the relative displacement and velocity between the rotor and stator, respectively, i is an integer between 0 and m, and $m > 1$.

The tangential stress $\hat{F}_t$ generated by the brake-friction material is

$$\hat{F}_t = \mu_{brk} \hat{F}_n \tag{4}$$

Consider the schematic representation of a four-wheel, main-landing gear truck shown in Fig. 3. Each wheel and brake are modeled as a single rotor and stator having the following degrees of freedom: Rigid-body lateral displacement and yaw of the stator and rotor (x_s, ϕ_s and x_r, ϕ_r, respectively); θ_s; and Ω_w.

For any point (r, θ) on the disk surface, the normal displacement and velocity are

$$x(r, \theta) = (x_s - x_r) - r \sin \theta(\phi_s - \phi_r) \tag{5}$$

$$\dot{x}(r, \theta) = (\dot{x}_s - \dot{x}_r) - r \sin \theta(\dot{\phi}_s - \dot{\phi}_r) \tag{6}$$

The normal force F_n from the normal contact stress is

$$F_n = \int_0^{2\pi} \int_{R_i}^{R_o} \hat{F}_n r \, dr \, d\theta \tag{7}$$

and the tangential force F_t generated by the brake-friction material is

$$F_t = \mu_{brk} F_n \tag{8}$$

The brake torque T is

$$T = \text{sgn}(\Omega_w - \dot{\theta}_s) \int_0^{2\pi} \int_{R_i}^{R_o} \mu_{brk} \hat{F}_n r^2 \, dr \, d\theta \tag{9}$$

The yawing moment M_b as a result of normal contact stress is

$$M_b = -\int_0^{2\pi} \int_{R_i}^{R_o} \hat{F}_n r^2 \sin \theta \, dr \, d\theta \tag{10}$$

Assume that the nonlinear contact stress $\hat{F}_n$ in Eq. (3) is represented by a cubic polynomial in the relative displacement only, i.e., $m = 3$. Then, substituting the expression for $x(r, \theta)$

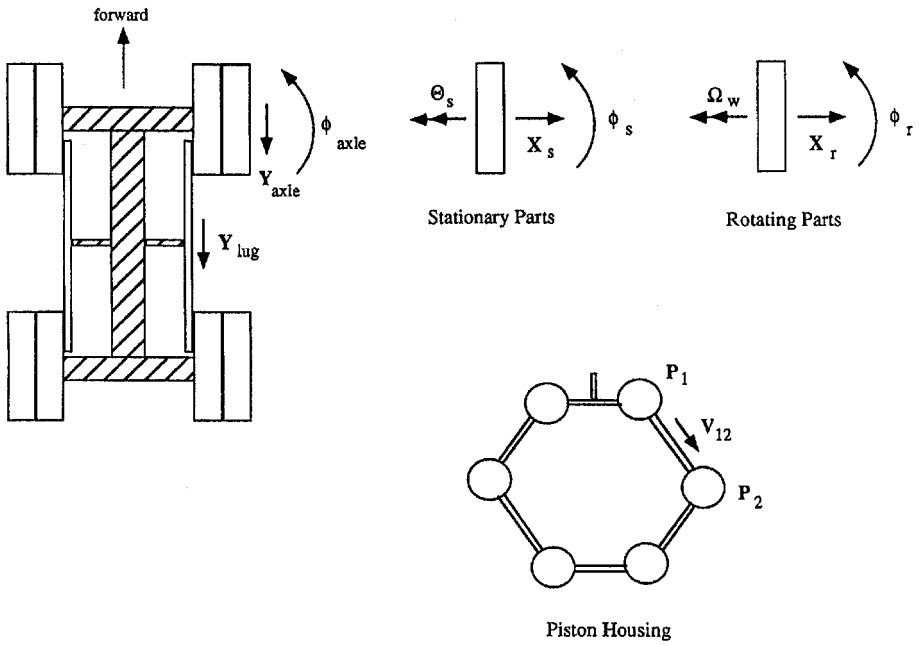

Fig. 3 Degrees of freedom.

from Eq. (5) into the expressions for F_n, T, and M_b in Eqs. (7), (9), and (10), yields

$$F_n = K_0A_2 + K_1A_2(x_s - x_r) + \tfrac{1}{4}A_4(\phi_s - \phi_r)^2[K_2 + 3K_3(x_s - x_r)] + A_2(x_s - x_r)^2[K_2 + K_3(x_s - x_r)] \quad (11)$$

$$M_b = -A_4(\phi_s - \phi_r)[\tfrac{1}{4}K_1 + \tfrac{1}{2}K_2(x_s - x_r)] - \tfrac{3}{4}K_3A_4(x_s - x_r)^2(\phi_s - \phi_r) - \tfrac{1}{8}K_3A_6(\phi_s - \phi_r)^3 \quad (12)$$

$$T = \operatorname{sgn}(\Omega_w - \dot{\theta}_s)\{\tfrac{2}{3}\mu_{brk}A_3[K_0 + K_1(x_s - x_r)] + \tfrac{2}{3}\mu_{brk}A_3(x_3 - x_r)^2[K_2 + K_3(x_s - x_r)] + \tfrac{1}{5}\mu_{brk}A_5(\phi_s - \phi_r)^2[K_2 + 3K_3(x_s - x_r)]\} \quad (13)$$

where

$$A_k = \pi(R_o^k - R_i^k), \qquad k = 2, 3, 4, 5, 6 \quad (14)$$

If the nonlinear contact stress $\hat{F}_n$ in Eq. (3) is represented by a cubic polynomial function of both the normal displacement $x(r, \theta)$ and velocity $\dot{x}(r, \theta)$, then additional terms will appear in the expressions for F_n, T, and M_b that are functions of the velocity variables ($\dot{x}_s$, $\dot{\phi}_s$, $\dot{x}_r$, and $\dot{\phi}_r$) and the coefficients C_i. These velocity variable terms will have the same functional forms as the displacement variable terms shown in Eqs. (11–13).

C. Brake Hydraulic Force

The brake net hydraulic force, which is determined by the net hydraulic pressure and the net piston area, is given by

$$F_{hyd} = P_{net}A_p \quad (15)$$

D. Brake-Rod Load

The brake-rod axial load F_{rod} is a function of θ_s, ϕ_s, y_{axle}, and y_{lug}. F_{rod} is given by

$$F_{rod} = \frac{K_\theta\theta_s}{R_e} - \frac{K_\theta d_e\phi_s}{R_e^2} + \frac{K_\theta(y_{axle} - y_{lug})}{R_e^2} \quad (16)$$

E. Slip Ratio

The tire slip ratio S is a function of v, y_{axle}, and Ω_w. It is defined to be

$$S = \frac{[(v - \dot{y}_{axle}) - \Omega_w R_r]}{(v - \dot{y}_{axle})} \quad (17)$$

When $\Omega_w R_r$ equals the net axle velocity $(v - \dot{y}_{axle})$, S is zero. When Ω_w equals zero, $S = 1.0$, which corresponds to 100% slip, the wheel is locked, and the tire skids.

F. Tire–Ground Drag Force

The tire–ground drag force is a function of W, S, and μ_{grd}, which is a nonlinear function of S. The drag force is given by

$$F_{drag} = W\mu_{grd} \quad (18)$$

μ_{grd} is an antisymmetric function of S.

$$\mu_{grd}(-S) = -\mu_{grd}(S) \quad (19)$$

G. Equations of Motion

The nonlinear-squeal equations of motion for a single brake are expressed in terms of the degrees of freedom x_s, ϕ_s, x_r, ϕ_r, θ_s, y_{axle}, ϕ_{axle}, y_{lug}, and Ω_w. The center-lug fore–aft deflection can be retained or neglected as desired.

The equations of motion are given in Eqs. (20–28). For the fore–aft wheel-pair model, the single-wheel degrees of freedom are included for each wheel plus the fore–aft deflection of the center lug y_{lug} on the landing-gear lower oleo strut, and the brake-rod loads from the fore and aft wheels. Equations of motion for models that include a flexible torque tube are presented in Appendix B

$$m_s\ddot{x}_s + C_{xs}\dot{x}_s + \mu_s|F_{rod}|\operatorname{sgn}(\dot{x}_s) = F_{hyd} - F_n \quad (20)$$

$$I_{\phi s}\ddot{\phi}_s + C_{\phi s}\dot{\phi}_s + K_{\phi s}\phi_s - F_{rod}d_e = +M_b \quad (21)$$

$$I_\theta\ddot{\theta}_s + C_\theta\dot{\theta}_s + F_{rod}R_e + \mu_{ph}|F_{rod}|R_b\operatorname{sgn}(\dot{\theta}_s) = T \quad (22)$$

$$m_r\ddot{x}_r + C_{xr}\dot{x}_r + \mu_r(|T|/R_w)\operatorname{sgn}(\dot{x}_r) + K_{rr}x_r = F_n \quad (23)$$

$$I_{\phi r}\ddot{\phi}_r + (C_{\phi r} + C_{wk})\dot{\phi}_r - C_{wk}\dot{\phi}_{axle} + K_{\phi r}\phi_r + K_{wk}(\phi_r - \phi_{axle}) = -M_b \quad (24)$$

$$m_{axle}\ddot{y}_{axle} + C_{yax}\dot{y}_{axle} + K_{11}y_{axle} + K_{12}\phi_{axle} = F_{drag} - F_{rod} \quad (25)$$

$$I_{axle}\ddot{\phi}_{axle} + (C_{\phi ax} + C_{wk})\dot{\phi}_{axle} - C_{wk}\dot{\phi}_r + K_{21}y_{axle} + K_{22}\phi_{axle} - K_{wk}(\phi_r - \phi_{axle}) = 0 \quad (26)$$

$$I_w\dot{\Omega}_w = -T + F_{drag}R_r \quad (27)$$

$$m_{lug}\ddot{y}_{lug} + C_{lug}\dot{y}_{lug} + K_{lug}y_{lug} - \sum F_{rod} = 0 \quad (28)$$

III. Coupling Mechanisms

The nonlinear contact stiffness of the brake heat-stack couples rotor and stator-rigid-body freedoms through the normal force, yaw moment, and torque, which are functions of the heat-stack relative displacement. It can be seen in Eqs. (11–13) that no coupling from F_n, M_b, and T would occur between the lateral displacement and yaw freedoms of the heat stack if the contact-stress relationship were linear, i.e., $K_2 = K_3 = 0$. These terms appear in the equations of motion (20–24) and (27).

The contact-stiffness and brake-friction terms (which are functions of rotor/stator lateral translation and yaw) are asymmetric in the linearized perturbation equations (given in Sec. IV) for an equilibrium point of the nonlinear system. This asymmetry gives rise to potential instabilities associated with these four degrees of freedom.

The geometry of the brake and landing-gear structure couples additional degrees of freedom, including, piston-housing torsional rotation, axle and center-lug fore–aft deflections, and heat-stack lateral translation and yaw caused by the brake-rod load terms in the equations of motion (20–22), (25), and (28). Additional coupling arises from the ground-drag force caused by tire slip at a low-slip ratio when the torque gain is positive. These two mechanisms and the coupling induced by the brake-friction material nonlinearities provide a complete feedback loop to the system.

It is the combination of the different coupling mechanisms that permits instability of the primary squeal mode. Both the geometric and asymmetric coupling, because of the brake-rod structural terms and the nonlinear contact-stress terms, respectively, must be present to produce the squeal-mode instability. Either of these coupling mechanisms alone is insufficient to adequately describe the primary-mode squeal phenomenon being modeled.

IV. Solution Methodology

The nonlinear squeal equations (20–28) have the form

$$[M]\{\ddot{\boldsymbol{x}}\} + [C]\{\dot{\boldsymbol{x}}\} + [K]\{\boldsymbol{x}\} = \{\boldsymbol{F}_{hyd}\} + \{\boldsymbol{F}_{damp}\} + \{\boldsymbol{F}_{disk}\} + \{\boldsymbol{F}_{drag}\} \quad (29)$$

where $\{\boldsymbol{x}\}$ is a vector of the time-dependent variables (degrees of freedom), $[M]$ is the inertia matrix, $[C]$ is the viscous damping matrix, and $[K]$ is the structural stiffness matrix. $[K]$ includes stiffness effects of all brake and landing-gear components excluding the brake-rotor and stator stiffnesses that are specified in $\{\boldsymbol{F}_{\text{disk}}\}$. The vector $\{\boldsymbol{F}_{\text{disk}}\}$ contains nonlinear contact stiffness terms caused by the relative displacements between brake rotors and stators. $\{\boldsymbol{F}_{\text{hyd}}\}$ is a vector of piston-hydraulic pressure terms. $\{\boldsymbol{F}_{\text{damp}}\}$ is a vector of nonlinear damping terms because of Coulomb friction. $\{\boldsymbol{F}_{\text{drag}}\}$ is a vector of terms because of the tire–ground drag load

$$\{\boldsymbol{x}\} = \{x_s \;\; \phi_s \;\; \theta_s \;\; x_r \;\; \phi_r \;\; y_{\text{axle}} \;\; \phi_{\text{axle}} \;\; \Omega_w \;\; y_{\text{lug}}\}^T \tag{30}$$

$$\{\boldsymbol{F}_{\text{hyd}}\} = \{F_{\text{hyd}} \;\; 0 \;\; 0 \;\; 0 \;\; 0 \;\; 0 \;\; 0 \;\; 0 \;\; 0\}^T \tag{31}$$

$$\{\boldsymbol{F}_{\text{drag}}\} = \{0 \;\; 0 \;\; 0 \;\; 0 \;\; 0 \;\; F_{\text{drag}} \;\; 0 \;\; R_r F_{\text{drag}} \;\; 0\}^T \tag{32}$$

$$\{\boldsymbol{F}_{\text{disk}}\} = \{-F_n \;\; M_b \;\; T \;\; F_n - M_b \;\; 0 \;\; 0 \;\; -T \;\; 0\}^T \tag{33}$$

$$\{\boldsymbol{F}_{\text{damp}}\} = \begin{Bmatrix} -\mu_s |F_{\text{rod}}| \operatorname{sgn}(\dot{x}_s) \\ 0 \\ -\mu_{\text{ph}} |F_{\text{rod}}| R_b \operatorname{sgn}(\dot{\theta}_s) \\ -\mu_r \dfrac{|T|}{R_w} \operatorname{sgn}(\dot{x}_r) \\ 0 \\ 0 \\ 0 \\ 0 \\ 0 \end{Bmatrix} \tag{34}$$

F_n, M_b, and T are given by Eqs. (11–13), respectively. F_{hyd}, F_{rod}, and F_{drag} are given by Eqs. (15), (16), and (18), respectively.

A. Steady-State Operating Point

For a given net-brake hydraulic pressure P_{net}, at equilibrium conditions, i.e., smooth sliding, the nonlinear equations satisfy the following conditions:

$$[K]\{\boldsymbol{x}_0\} = \{\boldsymbol{F}_{\text{hyd}}\} + \{\boldsymbol{F}_{\text{disk}}(x_0)\} \tag{35}$$

There can be more than one steady-state operating point at a given brake pressure because the squeal equations are nonlinear.

B. Stability Analysis

The first step in the solution procedure is to obtain the steady-state operating point for the full set of nonlinear squeal equations [Eq. (29)] by solving for the equilibrium point $\{\boldsymbol{x}_0\}$ in Eq. (35). There will be one or more operating points for the nonlinear systems being considered here. Stability of the system is investigated about each steady-state operating point by assuming small perturbations $\{\bar{\boldsymbol{x}}\}$ about the equilibrium point $\{\boldsymbol{x}_0\}$, where

$$\{\boldsymbol{x}\} = \{\boldsymbol{x}_0\} + \{\bar{\boldsymbol{x}}\} \tag{36}$$

$$\{\boldsymbol{x}_0\} = \{x_s \;\; \phi_s \;\; \theta_s \;\; x_r \;\; \phi_r \;\; y_{\text{axle}} \;\; \phi_{\text{axle}} \;\; \Omega_w \;\; y_{\text{lug}}\}_0^T \tag{37}$$

$$\{\bar{\boldsymbol{x}}\}^T = \{\bar{x}_s \;\; \bar{\phi}_s \;\; \bar{\theta}_s \;\; \bar{x}_r \;\; \bar{\phi}_r \;\; \bar{y}_{\text{axle}} \;\; \bar{\phi}_{\text{axle}} \;\; \bar{\Omega}_w \;\; \bar{y}_{\text{lug}}\}^T \tag{38}$$

Nonlinear damping terms caused by Coulomb friction in the piston-housing bushings are replaced by equivalent viscous damping in Eq. (29).

Substitution of Eq. (36) for small perturbations about the equilibrium point into the nonlinear squeal equations [Eq. (29)] and neglecting higher-order terms gives the linearized squeal equations of motion

$$[M]\{\ddot{\bar{\boldsymbol{x}}}\} + [C]\{\dot{\bar{\boldsymbol{x}}}\} + [K](\{\bar{\boldsymbol{x}}\} + \{\boldsymbol{x}_0\}) = \{\boldsymbol{F}_{\text{hyd}}\} + \{\boldsymbol{F}_{\text{disk}}(x_0)\} + \{\boldsymbol{F}_{\text{disk}}(\bar{x})\} + \{\boldsymbol{F}_{\text{drag}}(x_0)\} + \{\boldsymbol{F}_{\text{drag}}(\bar{x})\} \tag{39}$$

The force F_n, yaw moment M_b, and brake torque T because of normal contact stress are expressed in terms of both the equilibrium position $\{\boldsymbol{x}_0\}$ and the perturbation variables $\{\bar{\boldsymbol{x}}\}$, where

$$F_n(x) = F_n(x_0) + F_n(\bar{x}) \tag{40}$$

$$M_b(x) = M_b(x_0) + M_b(\bar{x}) \tag{41}$$

$$T(x) = T(x_0) + T(\bar{x}) \tag{42}$$

$$F_n(\bar{x}) = [K_1 A_2 + 2K_2 A_2 B_x](\bar{x}_s - \bar{x}_r) + \tfrac{1}{2} K_2 A_4 B_\phi (\bar{\phi}_s - \bar{\phi}_r) + K_3 (\bar{x}_s - \bar{x}_r)[3A_2 B_x^2 + \tfrac{3}{4} A_4 B_\phi^2] + \tfrac{3}{2} A_4 K_3 B_x B_\phi (\bar{\phi}_s - \bar{\phi}_r) + \cdots \tag{43}$$

$$M_b(\bar{x}) = -[\tfrac{1}{4} K_1 A_4 + \tfrac{1}{2} K_2 A_4 B_x](\bar{\phi}_s - \bar{\phi}_r) - A_4 B_\phi [\tfrac{1}{2} K_2 + \tfrac{3}{2} K_3 B_x](\bar{x}_s - \bar{x}_r) - \tfrac{3}{4} K_3 A_4 B_x^2 (\bar{\phi}_s - \bar{\phi}_r) - \tfrac{3}{8} K_3 A_6 B_\phi^2 (\bar{\phi}_s - \bar{\phi}_r) + \cdots \tag{44}$$

$$T(\bar{x}) = \tfrac{2}{3} \mu_{\text{brk}} A_3 [K_1 + 2K_2 B_x](\bar{x}_s - \bar{x}_r) + \tfrac{2}{5} \mu_{\text{brk}} K_2 A_5 B_\phi (\bar{\phi}_s - \bar{\phi}_r) + \mu_{\text{brk}} K_3 (\bar{x}_s - \bar{x}_r) \times [2A_3 B_x^2 + \tfrac{3}{5} A_5 B_\phi^2] + \tfrac{6}{5} \mu_{\text{brk}} K_3 A_5 B_x B_\phi (\bar{\phi}_s - \bar{\phi}_r) + \cdots \tag{45}$$

$$A_k = \pi (R_o^k - R_i^k), \qquad k = 2, 3, 4, 5, 6 \tag{46}$$

$$B_x = x_{s0} - x_{r0} \tag{47}$$

$$B_\phi = \phi_{s0} - \phi_{r0} \tag{48}$$

Note that constant terms proportional to K_0 or C_0 do not appear in Eqs. (43) or (45). They only enter into the steady-state operating point expressions for $F_n(x_0)$ and $T(x_0)$ given in Eqs. (11) and (13), respectively.

Stability analyses (eigensolutions) have been performed on the linearized squeal equations [Eqs. (39–48)] for small perturbations about an operating point of the nonlinear system. Results from these analyses are presented in a companion paper.[6] System instability is obtained for certain combinations of μ_{brk} and P_{net}, typically with high values of μ_{brk} and low levels of P_{net}. In general, the nonlinear contact-stiffness model predicts system instability at low-braking pressures and stability at high-braking pressures. Analysis results indicate that system instability can occur with a constant friction coefficient as has been observed frequently on both dynamometer and airplane tests. In general, stability decreases with increasing brake-fric-

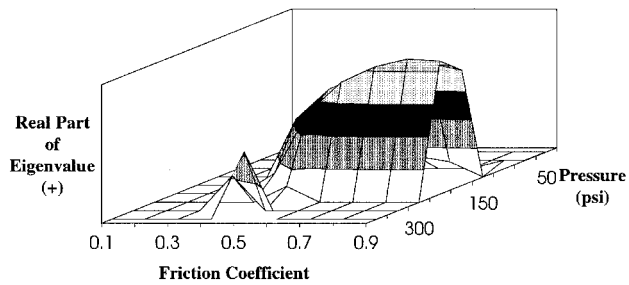

Fig. 4 Stability as a function of P_{net} and μ_{brk}.

tion coefficient. Typically, the system is stable at low values of μ_{brk} and unstable at high values.

A typical stability plot as a function of P_{net} and μ_{brk} is shown in Fig. 4. In this figure only the positive real part of the most unstable root is plotted. It is evident that stability, in general, is reduced by increasing friction coefficient and decreasing pressure.

C. Nonlinear Transient Analysis

Time-history response solutions have been obtained using a fourth-order Runge–Kutta algorithm to integrate the nonlinear squeal equations [Eqs. (20–28)]. Results from these analyses are also presented in a companion paper.[6] The response histories have been computed to complement the eigensolution results, evaluate stability of the nonlinear system near the operating points, evaluate stability of limit cycles and strange attractors, and determine response amplitudes, e.g., rod loads, accelerations, etc.

V. Summary and Conclusions

A model has been presented for the analysis of primary squeal-mode vibration in aircraft brake systems. The destabilizing mechanism in the model utilized mechanical and material surface properties of the brake heat stack to couple lateral translation and yaw of the rotors and stators. Geometric and stiffness properties of the brake and landing-gear structure couple piston-housing torsional rotation and axle fore–aft bending with lateral translation and twist of the heat stack.

The model does not use brake-negative damping and predicts that system instability can occur with a constant brake-friction coefficient as has been observed on both dynamometer and airplane tests. System stability can be altered by changes in the brake-friction coefficient, pressure, stiffness, geometry, and various brake-design parameters. Enhanced versions of the model were presented that include more detailed structural representation of the piston-housing torque tube and the hydraulic-flow equations for each piston. The model was extended to a fore–aft wheel pair on a two-axle, main-landing-gear truck.

Appendix A: Brake Hydraulic Equations

Continuity

$$\dot{p_i} = (B_i/V_i)(A_{L,i-1,i}V_{i-1,i} - A_{L,i,i+1}V_{i,i+1} - A_{p,i}\dot{S}_i) \quad \text{(A1)}$$

where

$$i = 1, \ldots 7 \quad \text{(A2)}$$

$$V_{67} = V_{60} \quad \text{(A3)}$$

Orifice

$$p_i - p_{i+1} = \frac{\rho A_{L,i,i+1}^2}{2(C_D A_{0,i,i+1})^2} V_{i,i+1}|V_{i,i+1}| + \rho L_{i,i+1}\dot{V}_{i,i+1} \quad \text{(A4)}$$

Continuity at Inlet

$$Q_0 + A_{L0}V_{60} = A_{L0}V_{01} \quad \text{(A5)}$$

$$p_0 - p_1 = \frac{\rho A_{L0}^2}{2(C_D A_{0,01})^2} V_{01}|V_{01}| + \rho L_{01}\dot{V}_{01} \quad \text{(A6)}$$

$$p_6 - p_0 = \frac{\rho A_{L0}^2}{2(C_D A_{0,60})^2} V_{60}|V_{60}| + \rho L_{60}\dot{V}_{60} \quad \text{(A7)}$$

$$\dot{S}_i = \dot{x}_s + \dot{\phi}_s r_p \sin\theta_i - \dot{x}_{ph} \quad \text{(A8)}$$

$$F_{hyd} = \sum_{i=1}^{6} p_i A_p \quad \text{(A9)}$$

$$M_{hyd} = \sum_{i=1}^{6} p_i A_p r_p \sin\theta_i \quad \text{(A10)}$$

Viscosity Effects

$$\Delta p = f(L/D)(\rho/2)V^2 \quad \text{(A11)}$$

where

$$f = C_f/N_R^{0.25} \quad \text{(A12)}$$

$$N_R = VD/\nu = \frac{\mu_d}{\rho} \quad \text{(A13)}$$

Hence

$$\Delta p = (\rho C_f L/2D^{1.25})V^{1.75} \quad \text{(A14)}$$

Appendix B: Torque-Tube/Axle Models

The equations of motion for the torque-tube model are given by

$$[M_{TT}]\{\ddot{\boldsymbol{x}}_{TT}\} + [C_{TT}]\{\dot{\boldsymbol{x}}_{TT}\} + [K_{TT}]\{\boldsymbol{x}_{TT}\} = \{\boldsymbol{F}_{TT}\} \quad \text{(B1)}$$

where

$$\{\boldsymbol{x}_{TT}\}^T = \lfloor y_1 \;\; \varsigma_1 \;\; y_2 \;\; \varsigma_2 \;\; y_3 \;\; \varsigma_3 \;\; y_4 \;\; \varsigma_4 \;\; y_5 \;\; \varsigma_5 \rfloor_{TT} \quad \text{(B2)}$$

$$\{\boldsymbol{F}_{TT}\} = \begin{Bmatrix} -F_{rod} \\ M_{rod} \\ -F_{PH} \\ -M_{PH} \\ -F_{TP} \\ -M_{TP} \\ 0 \\ M_{sp} \\ 0 \\ M_{bt} \end{Bmatrix} \quad \text{(B3)}$$

The $\{\boldsymbol{x}_{TT}\}$ degrees-of-freedom y_i and ς_i, $i = 1, 5$, are the fore–aft deflection and yaw rotation at the centerline of the brake rod (node 1); the centerline of the piston-housing bushing (node 2); the centerline of the torque-tube pedestal bushing (node 3); the c.g. of the heat stack (node 4); and the backing plate (node 5).

F_{rod} and M_{rod} are the force and moment exerted on the torque tube by the brake-rod axial load. F_{PH}, M_{PH}, F_{TP}, and M_{TP} are the force and moment at the center of the piston-housing and torque-tube pedestal bushings, respectively. M_{sp} is the moment caused by the relative bending angle between the torque tube and the stators. M_{bt} is the moment caused by the relative bending angle between the torque tube and the backing plate.

The axle equations of motion are given by

$$[M_{axle}]\{\ddot{\boldsymbol{x}}_{axle}\} + [C_{axle}]\{\dot{\boldsymbol{x}}_{axle}\} + [K_{axle}]\{\boldsymbol{x}_{axle}\} = \{\boldsymbol{F}_{axle}\} \quad \text{(B4)}$$

where

$$\{\boldsymbol{x}_{axle}\}^T = \lfloor y_1 \;\; \varsigma_1 \;\; y_2 \;\; \varsigma_2 \;\; y_3 \;\; \varsigma_3 \rfloor_{axle} \quad \text{(B5)}$$

$$\{\boldsymbol{F}_{axle}\}^T = \lfloor F_{PH} \;\; M_{PH} \;\; F_{TP} \;\; M_{TP} \;\; F_{drag} \;\; M_{bk} \rfloor \quad \text{(B6)}$$

The $\{\boldsymbol{x}_{axle}\}$ degrees-of-freedom y_i and ς_i, $i = 1, 3$, are the fore–aft deflection and yaw rotation at the centerline of the

piston-housing bushing (node 1); the centerline of the torque-tube pedestal bushing (node 2); and the wheel centerline (node 3).

F_{drag} and M_{bk} are the tire–ground drag force and the moment resulting from the relative bending angle between the axle and rotors. $\{\boldsymbol{F}_{drag}\}$ is a function of tire slip where $y_{axle} = y_{3axle}$ in Eq. (17) for S.

F_{rod} is given by

$$F_{rod} = K_{rod}R_e\theta_s - K_{rod}d_e\phi_s + K_{rod}(y_{axle} - y_{lug} + y_{1TT}) \quad \text{(B7)}$$

and the rod moment is to be either zero or a function of pin stiffness K_{pin}

$$M_{rod} = 0 \quad \text{(B8)}$$

or

$$M_{rod} = K_{pin}(\theta_{TT} - \varsigma_{1rod}) \quad \text{(B9)}$$

F_{PH}, M_{PH}, F_{TP}, and M_{TP} are given by

$$F_{PH} = K_{KPH}(y_{1axle} - y_{2TT}) \quad \text{(B10)}$$

$$M_{PH} = K_{MPH}(\varsigma_{1axle} - \varsigma_{2TT}) \quad \text{(B11)}$$

$$F_{TP} = K_{FTP}(y_{2axle} - y_{3TT}) \quad \text{(B12)}$$

$$M_{TP} = K_{MTP}(\varsigma_{2axle} - \varsigma_{3TT}) \quad \text{(B13)}$$

M_{bt}, M_{bk}, and M_{sp} are given by

$$M_{bt} = K_{bp}(\varsigma_{5TT} - \phi_{11}) \quad \text{(B14)}$$

$$M_{bk} = \sum_{i=2,4,\cdots}^{10} K_{bk}(\varsigma_{3axle} - \phi_i) \quad \text{(B15)}$$

$$M_{sp} = \sum_{i=1,3,\cdots}^{9} K_{sp}(\varsigma_{4TT} - \phi_i) \quad \text{(B16)}$$

where x_i and ϕ_i are the heat-stack axial displacement and yaw angle, respectively, and $i = 1$ (pressure plate), $i = 2$ (rotor 1), $i = 3$ (stator 1), $i = 4$ (rotor 2), and $i = 11$ (backing plate).

References

[1]Earles, S. W. E., and Soar, G. B., "Squeal Noise in Disc Brakes," *Symposium on Vibration and Noise in Motor Vehicles*, Proceedings Inst. of Mechanical Engineers, 1971, pp. 61–69.

[2]Ibrahim, R. A., "Friction-Induced Vibration, Chatter, Squeal, and Chaos, Part I: Mechanics of Contact and Friction," *Applied Mechanics Review*, Vol. 47, No. 7, 1994, pp. 209–226.

[3]Ibrahim, R. A., "Friction-Induced Vibration, Chatter, Squeal, and Chaos, Part II: Dynamics and Modeling," *Applied Mechanics Review*, Vol. 47, No. 7, 1994, pp. 227–253.

[4]Tworzydlo, W. W., Becker, E. B., and Oden, J. T., "Numerical Modeling of Friction-Induced Vibrations and Dynamic Instabilities," *Friction-Induced Vibration, Chatter, Squeal, and Chaos*, Vol. DE-Vol. 49, *Proceedings of the ASME Winter Annual Meeting*, American Society of Mechanical Engineers, New York, 1992, pp. 13–32.

[5]Millner, N., "An Analysis of Disc Brake Squeal," Society of Automotive Engineers, Paper 780332, New York, 1978.

[6]Gordon, J. T., Liu, S. Y., and Özbek, M. A., "Nonlinear Model for Aircraft Brake-Squeal Analysis: Stability Analysis and Parametric Studies," *Journal of Aircraft*, Vol. 35, No. 4, 1998, pp. 631–636.